Carbon 152 (2019) 451–458

Contents lists available at ScienceDirect

Carbon

journal homepage: www.elsevier.com/locate/carbon

The intrinsic temperature-dependent Raman spectra of graphite in the temperature range from 4K to 1000K

H.-N. Liu [a, b, c, 1], X. Cong [a, b, 1], M.-L. Lin [a, b], P.-H. Tan [a, b, *]

[a] State Key Laboratory of Superlattices and Microstructures, Institute of Semiconductors, Chinese Academy of Sciences, Beijing, 100083, China
[b] Center of Materials Science and Optoelectronics Engineering, University of Chinese Academy of Sciences, Beijing, 100049, China
[c] Key Laboratory of Opto-Electronic Information Technology of Ministry of Education, School of Precision Instrument and Opto-Electronics Engineering, Tianjin University, Tianjin, 300072, China

ARTICLE INFO

Article history:
Received 11 February 2019
Received in revised form
4 May 2019
Accepted 7 May 2019
Available online 11 May 2019

ABSTRACT

Temperature-dependent (T-dependent) Raman scattering can provide valuable informations on thermal properties, phonon anharmonicity and electron-phonon coupling of graphene-based materials. Graphene are found to exhibit extrinsic T-dependent Raman behavior at low temperature in vacuum or N_2 gas, showing a behavior of heavily doped graphene. To obtain intrinsic properties of graphene-based materials, we focused on the comparative T-dependent Raman study on graphite and silicon in the temperature range of 4 K~1000 K by different excitation lasers and different hot-stages or cryogenic stations. In contrast to the monotonic increase of full width at half maximum (FWHM) with temperature for the Si mode in silicon, FWHM for the G mode in graphite exhibits a minimum when $T \sim 700K$, which can be explained by the contributions from phonon anharmonicity and electron-phonon coupling. The result shows that the previous theoretical works underestimate the contribution from phonon anharmonicity above ~ 600 K. The electron-phonon coupling strength of 0.026 is revealed, smaller than that of graphene. The peak position of G peak of graphite shows a nonlinear decrease with increasing temperature, which agrees well with the previous theoretical calculation. Our results find that the contribution of phonon anharmonicity to both peak position and FWHM is more prominent for the G mode in graphite than the Si mode in silicon.

1. Introduction

Raman scattering is one of widely used techniques to characterize the phonon properties of condensed matters [1,2]. The temperature-dependent (T-dependent) line width and peak shift of a Raman mode can provide valuable information about anharmonic terms in the lattice potential energy and the electron-phonon coupling (EPC) of the corresponding phonons in condensed matters [3]. Graphene is nowadays widely studied to use in novel electronic and photonics applications [4,5], since they demonstrated superior properties including thermal transport and conductance, ballistic transport, high mobility and electrical conductance [6–10]. It is indispensable to study the phonon anharmonicity and EPC of graphene to obtain an in-depth understanding of the above properties. There are many works about the temperature effect of Raman experiments on graphene flakes [11–17]. However, there exists apparent inconsistency between experiments from different groups. Linas et al. [13] found a nonlinear behavior of the peak position of the G peak, Pos(G), versus temperature for graphene, which is grown using chemical vapor deposition (CVD) technique and transferred onto SiN substrate. Lee et al. [16], on the other hand, found that for a CVD-grown graphene on Cu foil, Pos(G) showed a linear decrease with increasing temperature. Many works notice that the ultrathin nature of graphene makes the effect of substrate pivotal to understand its T-dependent Raman spectra. Due to the mismatch between the thermal expansion coefficient (TEC) of graphene and substrate, when temperature varies, there will be strain [12–15] between the substrate and graphene layer. Tian et al. [15] found that mechanically exfoliated graphene shows a similar T-dependent Pos(G) no matter whether the graphene has been suspended or transferred onto Si/SiO_2 substrate. Shaina et al. [14], on the other hand, found that for the wet-transferred CVD-grown

* Corresponding author. State Key Laboratory of Superlattices and Microstructures, Institute of Semiconductors, Chinese Academy of Sciences, Beijing, 100083, China.
E-mail address: phtan@semi.ac.cn (P.-H. Tan).
[1] These authors contributed equally to this work.

https://doi.org/10.1016/j.carbon.2019.05.016
0008-6223/

graphene, the T-dependent Pos(G) of graphene with the copper, SiO_2/Si or PDMS substrates are different. These works show that dopants, defects in the material, as well as growth method, could lead to different temperature dependence in the Pos(G) of graphene.

To clarify why there exists apparent inconsistency between experiments of graphene samples from different groups, we performed Raman measurement of the mechanically exfoliated graphene on SiO_2/Si substrates under different experimental conditions, as demonstrated in the section of experimental methods. The corresponding results are shown in Fig. 1. Note that the choice of sample excludes the influence of factors such as charged impurities, disorder and doping which possibly leads to a large variation of Pos(G) and full width at half maximum of G mode (FWHM(G)) [2,18]. Therefore, *all the as-exfoliated graphene flakes for Raman measurements in this work were chosen to exhibit Pos(G) of ~ 1582 cm^{-1} within the whole flake, a typical Pos(G) for pristine and undoped graphene.* [2,19] It is found that when the graphene sample is sealed at a vacuum of 10^{-8} mbar, its Pos(G) can dramatically increase from 1582 cm^{-1} to 1591 cm^{-1} at room temperature in some cases, as shown in Fig. 1 (a). When the sample was cooled down to 80 K, its Pos(G) was linearly increased up to 1596 cm^{-1} with a slope of -0.0238 cm^{-1}/K. When the sample was heated from 80 K to 400 K, Pos(G) follows the trace of the cooling process but significantly diverges from the linear dependence when the sample is above room temperature, as shown by point-down and point-up triangles in Fig. 1(b). Even by the same nitrogen cooled cryogenic station, we found that two experiments can show quite different T-dependent Pos(G), as shown by point-up triangles and diamonds in Fig. 1(b). Fig. 1(c) summarized the typical T-dependent Pos(G) at different conditions from many measurements. It turns out that, although the as-exfoliated flake is pristine graphene, the variation of Pos(G) can be as large as 9 cm^{-1} under different experimental conditions at specific temperature. Because the slight and moderate doping can make Pos(G) of graphene upshift at specific temperature [20], the large variation of Pos(G) up to 9 cm^{-1} means that the samples exhibit different doping levels at different experimental conditions. This may be one of the major reasons for the large variation of Pos(G) of graphene dependent on temperature reported by different groups [11–16]. FWHM(G) is very sensitive to the doping level of graphene (i.e., its Fermi energy E_F) [2,18,20–22]. However, T-dependent FWHM(G) of intrinsic graphene is barely reported. Fig. 1(d) summarizes the FWHM(G) of the corresponding experiments in Fig. 1(c) at different conditions and by different instruments. Although FWHM(G) of the exfoliated graphene flakes is ~ 13 cm^{-1}, the measured FWHM(G) in vacuum or in the N_2 gas environment at different temperatures is significantly sharpened down to 6~9 cm^{-1}. This confirms that the graphene sample is heavily doped when it is sealed in vacuum or in the N_2 gas environment, leading to that FWHM(G) is not sensitive to temperature. The FWHM(G) sharpening is due to blockage of the phonon decay into electron-hole pairs due to the Pauli exclusion principle, when the electron-hole gap becomes higher than the phonon energy [18,21,22]. Variation of FWHM(G) in different experiments confirms that the measured T-dependent FWHM(G) are not from the intrinsic graphene. Therefore, in the further Raman experiments to clearly reveal the intrinsic phonon anharmonicity and EPC in graphene, it is very important to confirm that the graphene sample keeps pristine and undoped at all the measurement temperatures.

By reviewing the previous work, as well as performing T-dependent Raman measurements by ourselves, we come to realize that there are several inevitable factors that influence the Raman spectra of the graphene system. First, the Raman spectra can be dependent on sample in the presence of defects, doping and adsorbate. Second, graphene flakes grown by different techniques also exhibits different Raman features even at room temperature.

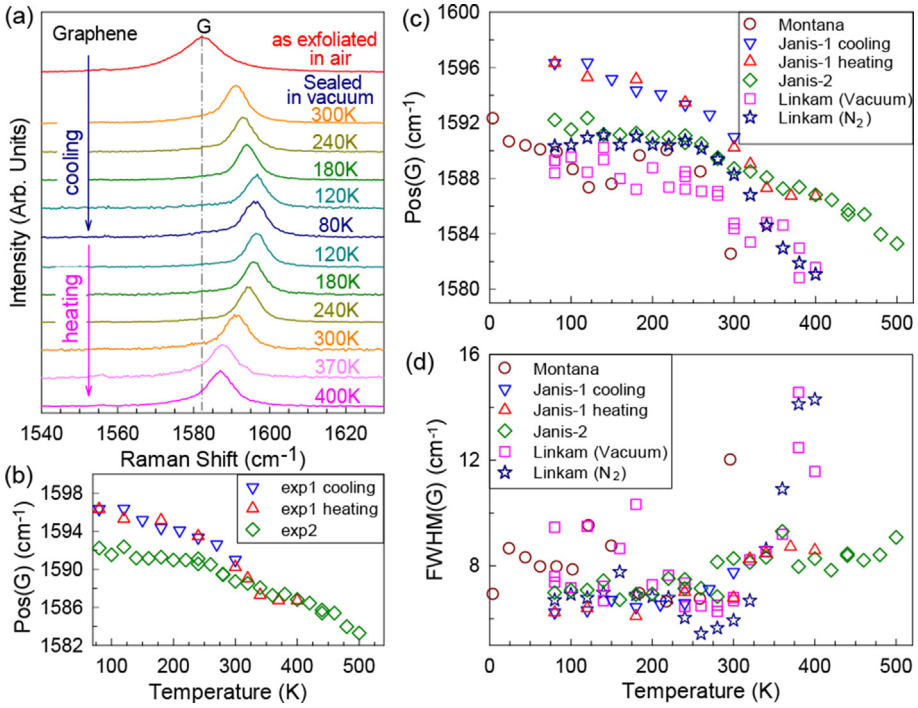

Fig. 1. (a) Raman spectrum of the G mode of as-exfoliated pristine graphene in air, and those sealed in vacuum when the sample was cooled from room temperature down to 80 K and then heated from 80 K up to 400 K. (b) T-dependent Pos(G) of the graphene sample (exp1) in (a) and another graphene sample (exp2) measured by the same nitrogen cooled cryogenic station. (c) T-dependent Pos(G) and (d) FWHM(G) of graphene samples when they are measured by different systems and different experimental conditions. $\lambda_{ex} = 514$ nm. (A colour version of this figure can be viewed online.)

Third, the detailed experimental condition for Raman measurements, such as placing the graphene flakes in vacuum, or nitrogen atmosphere as shown by Fig. 1, may also influence the resultant Raman spectra. Forth, the ultrathin nature of graphene makes it a prerequisite to always consider the TEC mismatch between the material and the substrate. The calculated TEC of graphene, however, exhibits considerable different T-dependent behaviors when using different calculation techniques or settings [23–26]. This makes it difficult to extract the intrinsic T-dependent Pos(G) from Raman measurement of graphene on substrate. In short, it seems that both the experimental and theoretical works on T-dependent Raman spectrum of graphene cannot reach a coincident result, which hinders the intrinsic temperature effect of graphene to be revealed.

Graphite can be considered as a nontrivial prototype to study the intrinsic temperature effect of graphene-based materials based on the following reasons: 1) Graphite is a semi-metal material formed by stacking numbers of graphene layers along c-axis, thus its phonon anharmonicity and EPC should be closely related to that of graphene. 2) In contrast to graphene, graphite is more stable, lacks charged impurities, and shows very low sensitivity to variations in experimental setup. 3) Its TEC had been well studied. 4) Graphite is too thick to consider any strain effect from substrate.

Although the Raman spectra of graphite has been studied for about 45 years [27], there are a few studies on temperature revolution for the G modes in graphite in detail [28–31]. The whole picture of temperature dependence is well understood by theory [3]. It is very important to determine the intrinsic values of the related parameters for its applications in fundamental research. However, the intrinsic contribution from EPC and phonon anharmonicity has not been distinguished for FHWM(G) in graphite by experiments up to now. For example, the probed FWHM(G) at room temperature by UV excitation [31] is as large as 16 cm^{-1}, and the frequency variation around specific temperature is as large as ~ 1.0 cm^{-1}. In the fitting, the theoretical value of EPC term [3] is directly used, resulting in the phonon anharmonicity contribution at T = 0 K being as large as ~4 cm^{-1}, much larger than the corresponding theoretical value of 1.6 cm^{-1} [3]. P. Giura et al. reported temperature evolution [30] of the G mode in graphite in the temperature range of 300–700 K. The theoretical and experimental data were presented without fitting to distinguish the contributions from EPC and phonon anharmonicity. Both of the two works do not declare the subtraction of the spectral broadening of Raman system from the experimental data, which may lead to large error in the determination of intrinsic contribution from EPC and phonon anharmonicity. Because FWHM(G) in graphite is mainly determined by EPC contribution, not so sensitive to temperature in comparison to other semiconductors, like silicon [32], the Raman system with high spectral resolution and the measurement below room temperature are necessary. Therefore, more works are needed to further understand the T-dependent evolution of FWHM(G) in graphite.

In this work, we investigate the T-dependent Raman spectra of bulk graphite in the temperature range of 4–1000 K. We use Raman system with a high spectral resolution of 0.45 cm^{-1}, two laser excitations and three independent hot-stages to confirm the experimental data to be reliable and repeatable. Most importantly, to obtain intrinsic fitting parameters from the experimental works, the spectral broadening from Raman system was excluded from the experimental data. Unlike graphene, the Raman spectra of which show significant dependence on the instruments used and the experimental conditions, graphite show similar T-dependent Raman behavior for different experimental conditions and different excitations. This ultimately enables us to reveal the intrinsic temperature effect of bulk graphite on its G modes and to distinguish the contribution of phonon anharmonicity and EPC to FWHM(G) without any ambiguity. Pos(G) and Pos(2D) of graphite decrease nonlinearly with temperature in the range of 4 ~ 1000 K. FWHM(G) decreases with temperature up to 700 K and then increases with temperature, in contrast to that of the 2D mode which linearly increases with temperature. Because FWHM(G) is mainly determined by the EPC term, the contribution from phonon anharmonicity is expected to be weak. However, the comparative study of graphite and silicon shows that the contribution of phonon anharmonicity to the G mode in graphite is more prominent than the Si mode in silicon.

2. Experimental methods

The graphite samples are standard highly oriented pyrolytic graphite for achieving the atomic image of graphite layer in scanning tunneling microscope systems (Park Scientific Instruments). Monolayer graphenes were obtained by micromechanical cleavage of natural graphite on the surface of a Si wafer chip with 90-nm-thick SiO_2 on the top [33], which are identified by Raman spectroscopy and optical contrast measurement [34].

The Raman measurements were performed in back-scattering geometry using a Jobin-Yvon HR800 system equipped with a liquid nitrogen cooled charge-coupled detector. The excitation wavelengths λ_{ex} are 514.5 nm from an Ar^+ laser and 632.8 nm from a He–Ne laser. Using a grating with a groove density of 1800/mm, the achieved spectral resolution were 0.45 cm^{-1}. A long working distance 50 × objective lens were used to ensure high signal to noise ratio, achieving a spatial resolution better than 0.7 μm. During all the measurements, laser power has been kept low enough to prevent any sample heating. The broadening from Raman system is estimated to be ~ 1.1 cm^{-1} based on the measurement of the Rayleigh signal at 0.0 cm^{-1}.

To obtain the T-dependent Raman spectra of graphene under different conditions, four systems have been used: a helium cooled cryogenic station (Montana Instruments) covering the temperature range from 4 K to 300 K at a vacuum of 10^{-1} mbar, two programmable hot-stages THMS600 and THMS350V (Linkam Scientific Instruments) covering the temperature range, respectively, from 80 K to 1000 K in a N_2 gas environment and from 80 K to 600 K at a vacuum of 10^{-3} mbar, and a Nitrogen cooled cryogenic station ST400-UHV (Janis Research Co.) covering the temperature range from 80 K to 500 K at a vacuum of 10^{-8} mbar. Both of the two Linkam instruments have a temperature stability of 0.1 K.

A 514 nm laser has been used as the major excitation source to conduct measurements covering the temperature range from 4 K to 300 K by Montana system and from 300 K to 1000 K by TS1200 stage (Linkam Scientific Instruments). A 633 nm laser has also been used as an additional excitation source to measure Raman spectra of graphite by THMS600 from 80 K to 800 K, aiming to further confirm the results by the 514 nm laser.

3. Results and discussions

Fig. 2 (a) and (b), respectively, show the typical spectral feature of the G and 2D modes of graphite: the former could be well fitted by a single Lorentzian peak, and the latter by double Lorentzian peaks (notated as $2D_1$ and $2D_2$ peak, respectively) [35]. Fig. 2(c) and (d) present the T-dependent G and 2D modes in the form of contour plots in the range from 4 K to 1000 K, showing the Raman intensities of the G and 2D modes versus frequency and temperature. The peak intensity of each spectrum was normalized to 1 to conduct direct comparison regarding the FWHM of different modes. For a comparison purpose, the typical spectral feature of the Si mode at 521 cm^{-1} in silicon at room temperature and its contour

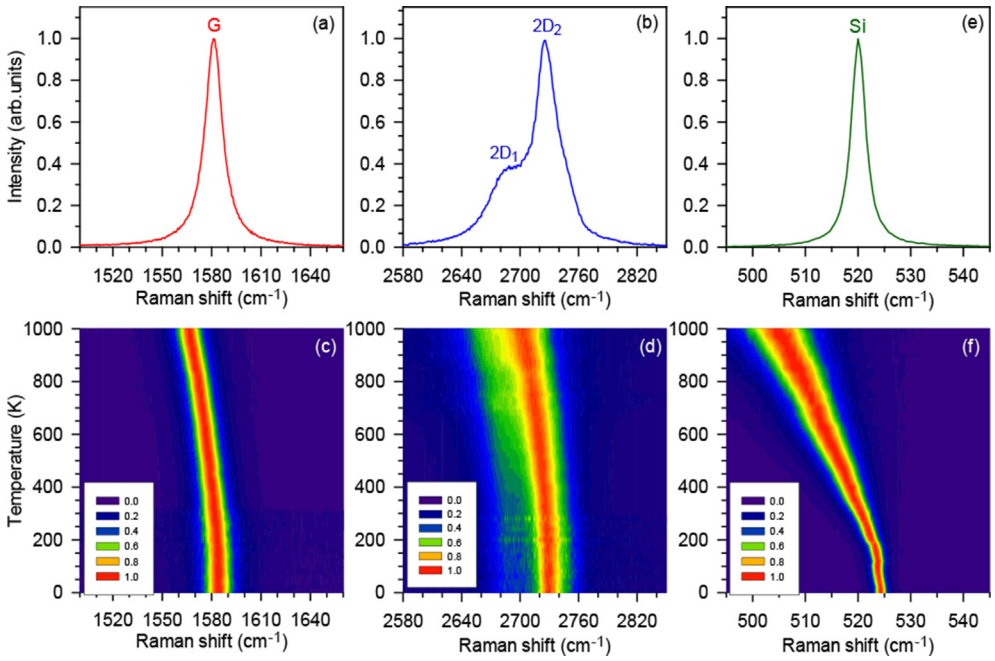

Fig. 2. Raman spectra of the (a) G and (b) 2D modes in graphite, and the corresponding contour plot of Raman intensity of the (c) G and (d) 2D modes versus frequency and temperature. For comparison, Raman spectrum of (e) the optical mode (Si mode) at ~ 521 cm^{-1} in silicon and (f) the corresponding contour plot are shown. $\lambda_{ex} = 514$ nm. (A colour version of this figure can be viewed online.)

plot of T-dependent Raman spectra are also presented in panels (e) and (f) of Fig. 2, respectively. Inspecting on the contour plots shown in panels (c), (d) and (f), the FWHM of the three modes exhibits different T-dependent behaviors. As temperature increases, the Raman mode of silicon shows the most obvious broadening, from 1.7 cm^{-1} at 4 K to 9.7 cm^{-1} at 1000 K. For the 2D mode in graphite, FWHM($2D_1$) and FWHM($2D_2$) are also broadened with a smaller increase rate. In addition, the relative intensity of the $2D_1$ peak increases with temperature, leading to the 2D mode becoming much broader at higher temperature. In contrast to the 2D and Si modes, however, the G mode in graphite does not show any noticeable broadening as the temperature increases from 4 K to 1000 K.

Before delving into the detailed discussion on the T-dependent FWHM of the Raman modes in graphite and silicon, we firstly go through the mechanisms that make contributions to the FWHM broadening. For a perfect sample free of doping, defects and disorders, phonons can decay into lower-energy phonons (ph-ph) or by creating an electron-hole pair (e-ph). Therefore, the corresponding Raman mode have a finite T-dependent FWHM, $\Gamma(T)$, which includes the following two terms [3]:

$$\Gamma(T) = \Gamma^{an}(T) + \Gamma^{EPC}(T) \tag{1}$$

where Γ^{an} represents the contribution from phonon-phonon interactions due to anharmonicity in lattice vibrational potentials and Γ^{EPC} represents the contribution from the EPC term of the Raman mode. Γ^{an} could be determined by considering scattering processes together with three phonons (3-ph) and four phonons (4-ph) and expressed by the following equation [32]:

$$\Gamma^{an}(T) = A\left[1 + 2f_{an}\left(\frac{x}{2}\right)\right] + B\left[1 + 3f_{an}\left(\frac{x}{3}\right) + 3f_{an}^2\left(\frac{x}{3}\right)\right] \tag{2}$$

where $x = \hbar\omega_0/(k_BT)$, $f_{an}(x) = 1/[(exp(x) - 1)]$, A and B are fitting constants, ω_0 is the phonon frequency at T=0K and k_B is the Boltzmann constant. $f_{an}(x)$ terms describe phonon population at thermal equilibrium in Bose-Einstein distribution. On the other hand, Γ^{EPC} is present in a system with null electron gap, the situation of which applies to pristine graphite with $E_F = 0$. In this case, this term could be modeled by the following equation [3]:

$$\Gamma^{EPC}(T) = \Gamma^{EPC}(0)\left[f_{epc}(-x/2) - f_{epc}(x/2)\right] \tag{3}$$

where $x = \hbar\omega_0/(k_BT)$ and $f_{epc}(x) = 1/[\exp(x)+1]$ is the Fermi-Dirac distribution at temperature T. $\Gamma^{EPC}(0) = \frac{\lambda_\Gamma}{4}\omega_0$, in which λ_Γ is a dimensionless coefficient corresponding to the EPC strength [3] at the Γ point. Such variation of Γ^{EPC} in graphite is due to the decay of the G phonon into an electron-hole pair. For a material with visible or near-infrared bandgap, e.g., silicon, the contribution of Γ^{EPC} to FWHM can be ignored.

Fig. 3(a) and (b) show the T-dependent FWHM($2D_2$) and FWHM(G), respectively. In Fig. 3(b), blue diamonds are FWHM measured by the Montana station (4~300 K) and TS1200 stage (300~1000 K) with $\lambda_{ex} = 514.5$ nm, and pink circles are FWHM measured by the THMS600 stage (80~800 K) with $\lambda_{ex} = 633$ nm. Note that the data shown in these two panels are obtained by subtracting the spectral broadening (~ 1.1 cm^{-1}) of Raman system from the experimental data. As shown in Fig. 3(a), FWHM($2D_2$) exhibits a linear dependence on temperature, with a slope of 0.012 cm^{-1}/K and an intercept of 28.1 cm^{-1} at 0 K for $\lambda_{ex} = 514$ nm. For the G mode, FWHM(G) does not show the dependence on λ_{ex} in the visible range. Thus, two λ_{ex} (514.5 nm and 633 nm) were used to confidently confirm the weak T-dependent FWHM(G) of graphite, as depicted in Fig. 3(b) by blue diamonds and pink circles, respectively. Interestingly, different from a monotonic variation of FWHM(G) with increasing temperature, FWHM(G) demonstrates a more intriguing behavior: it firstly decreases with a quite small rate until 700 K, then slowly increases afterwards. To understand this peculiar T-dependent behavior, Eq. (1) is used to fit the data of FWHM(G), as shown by the red solid line in Fig. 3(b). The red solid line achieves a perfect fitting for the experimental results. At the

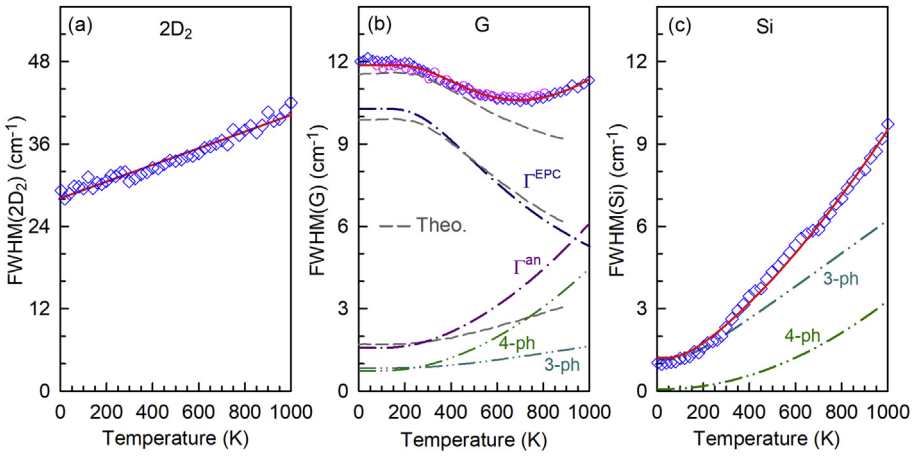

Fig. 3. The experimental T-dependent FWHM for the (a) 2D and (b) G modes of graphite, and (c) the optical mode of silicon. In (b), the sum of EPC and phonon anharmonicity (dash-dotted lines) contributions can provide a good fit (the solid line) to the experimental FWHM(G), and the fitted parameters are $A = 0.84\ cm^{-1}$, $B = 0.74\ cm^{-1}$ and $\Gamma^{EPC}(0) = 10.3\ cm^{-1}$. The theoretical FWHM(G) and the corresponding EPC and phonon anharmonicity contributions [3] are indicated by gray dashed lines. In (c), the experimental FWHM(Si) can also be well fitted by the 3-ph and 4-ph contributions based on Eq. (2), and the fitted parameters are $A = 1.15\ cm^{-1}$ and $B = 0.07\ cm^{-1}$. The dash-dot-dotted lines in (b) and (c) show the 3-ph and 4-ph contributions to the experimental FWHM(G) and FWHM(Si), respectively. Note that $1.1\ cm^{-1}$ was subtracted from the experimental FWHM to account for the system broadening. (A colour version of this figure can be viewed online.)

same time, the contribution from the anharmonicity and EPC are also depicted separately using dash-dotted lines. The EPC contribution dominates on the overall profile until 700 K, which leads to a general decreasing profile. On the other hand, the contribution from the phonon anharmonicity is increasing with temperature, leading to an increasing profile after 700 K which could not be fully compensated by the EPC contribution. At T = 0 K, $\Gamma^{an}(0) = 1.58\ cm^{-1}$ and $\Gamma^{EPC}(0) = 10.3\ cm^{-1}$. These values agree well with the calculated ones by first principle theory [3], being $1.65\ cm^{-1}$ and ~ $9.8\ cm^{-1}$, respectively. The experimental $\Gamma^{EPC}(0)$ gives $\lambda_\Gamma = 0.026$, which is slightly smaller than that (0.032) of graphene [36] and slightly larger than the value (0.025) of graphite [3]. However, we notice that the experimental $\Gamma^{an}(T)$ is much larger than the theoretical results [3] above 600 K, leading to an upward profile in Γ(T) at high temperature side, which diverges from the case of the theoretical work [3].

The T-dependent FWHM(Si) of silicon is shown in Fig. 3(c). Since the electron gap in silicon is much larger than energy of related phonon, the contribution from EPC is excluded. The solid line shows a very good fit by considering the contributions from the phonon anharmonicity involving 3-ph and 4-ph scattering processes, as depicted by the two dash-dotted lines [32]. The fitting indicates that the 3-ph scattering process dominates the T-dependent FWHM(Si). As temperature increases, the contribution from the 4-ph scattering process become more and more important. It is interesting that comparing Γ^{an} in graphite and silicon, Γ^{an} is expected to be small in graphite, and the theoretical contribution of $\Gamma^{an}(900\ K)$ to FWHM(G) is only $3\ cm^{-1}$ [3]. However, the fitted contribution $\Gamma^{an}(900\ K)$ is close to $5.0\ cm^{-1}$, which is comparable to $8.3\ cm^{-1}$ of $\Gamma^{an}(900\ K)$ in silicon. Therefore, the results reveal that phonon anharmonicity contribution to FWHM(G) is dominant in graphite at temperature above 900 K.

Fig. 4(a) and (b) depict Pos(G) and Pos($2D_2$) as a function of temperature. In Fig. 3(a), Pos(G) obtained by using 514.5 nm (blue open diamonds) and 633 nm laser (pink open circles) are presented together. Previous reports in graphite, graphene and nanotubes observed a linear dependence of the peak position [11,15,28,30,37,38]. However, here both the two peaks demonstrate a nonlinear dependence of the peak position on temperature. For instance, the temperature coefficients of the G ($2D_2$) peak are −0.0127 (−0.0122), −0.0170 (−0.0247), −0.0201 (−0.0312), and −0.0260 (−0.0406) cm^{-1}/K, respectively, in the temperature ranges of 80~300 K, 300~500 K, 500~700 K, and 700~900 K. Taking the G mode for an instance, at high temperature side, the temperature coefficient of peak position is more than two times as that of low temperature side.

The dependence of peak positions on temperature, $\omega(T)$, could be attributed mainly to two factors by the following equation:

$$\omega(T) = \omega_0 + \Delta\omega^{thermal}(T) + \Delta\omega^{an}(T) \tag{4}$$

where $\Delta\omega^{thermal}(T)$ accounts for the variation of the harmonic pulsation by varying the lattice parameters (as a consequence of the thermal expansion) and can be calculated by the following equation [39]:

$$\Delta\omega^{thermal}(T) = \omega_0 exp\left\{ -\eta\gamma_G \int_0^T \alpha(T')dT' \right\} \tag{5}$$

where γ_G is the Grüneisen constant, $\alpha(T)$ is the linear T-dependent expansion coefficient of the material and η is the dimensionality factor of the material ($\eta = 2$ for the G mode in graphite and $\eta = 3$ for the Si mode in silicon). The $\Delta\omega^{an}(T)$ term in Eq. (4) can be interpreted as anharmonic contribution involving 3-ph and 4-ph scattering processes and expressed by the following equation [32]:

$$\Delta\omega^{an}(T) = C\left[1 + 2f_{an}\left(\frac{x}{2}\right)\right] + D\left[1 + 3f_{an}\left(\frac{x}{3}\right) + 3f_{an}^2\left(\frac{x}{3}\right)\right] \tag{6}$$

where C and D are fitting constants, $x = \hbar\omega_0/(k_B T)$ and $f_{an}(x) = 1/[\exp(x) - 1]$, as mentioned in Eq. (2). However, taking Eq. (5) and Eq. (6) into Eq. (4) to fit T-dependent Pos(G), it exhibits obvious difference between experimental and fitted results. Indeed, in the previous works [3,30], all the terms in Eq. (4) for graphite as addressed above had been calculated by density functional theory, including the contribution from the 3-ph and 4-ph scattering processes. The total theoretical contributions from expansion and phonon anharmonicity [3] are depicted by the solid line in Fig. 4(a). It is shown that except for some small discrepancy in the range of 4~70 K (the maximum of the discrepancy goes to around $0.8\ cm^{-1}$ at 20 K), the experimental results are in very good

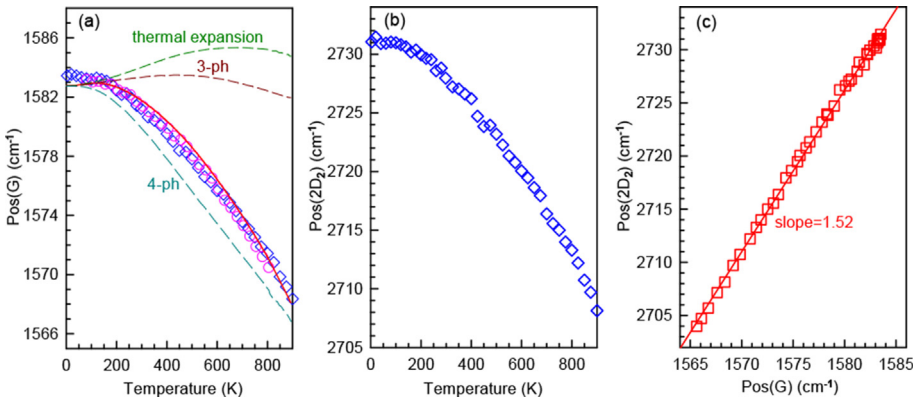

Fig. 4. T-dependent (a) Pos(G) and (b) Pos($2D_2$) of graphite. In panel (a), the solid line provides the total theoretical Pos(G) by considering the contributions from thermal expansion and phonon anharmonicity (including 3-ph and 4-ph scattering processes) [3]. The individual contributions (dashed lines) are also depicted by appropriately offsetting the according data. (c) Correlation between Pos(G) and Pos($2D_2$) of graphite at different temperatures. (A colour version of this figure can be viewed online.)

consistency with the theoretical ones [3]. To compare the contributions from 3-ph, 4-ph scattering processes and thermal expansion, these three contributions are also depicted separately by dashed lines in Fig. 4(a), by offsetting the contributions accordingly. The thermal expansion and the 3-ph scattering process generally lead to a positive line shift, while the 4-ph scattering process leads to a negative line shift. Among these three factors, the 3-ph scattering process gives the smallest contribution, while the 4-ph scattering process dominates the overall contribution. Indeed, the theoretical contributions from 3-ph and 4-ph scattering processes can not be fitted by the corresponding parts in Eq. (6).

As for the 2D mode, its peak position is also nonlinearly dependent on temperature. However, it is not proper to use 3-ph and 4-ph scattering processes to account for the contributions from the anharmonicity. More work is needed to explain its T-dependent behavior, which is beyond the scope of this work. The correlation between Pos($2D_2$) and Pos(G) of graphite at different temperatures is depicted in Fig. 4(c). The slope $\partial Pos(2D_2)/\partial Pos(G)$ is 1.52, much smaller than the ratio (1.72) between Pos($2D_2$) and Pos(G). The temperature variation can result in the lattice change to modify the phonon dispersion curve of graphite. The band structure of graphite is also dependent on temperature. Pos($2D_2$) is determined by the double resonant Raman process [40,41], which is sensitive to the band structure of graphite, thus, it is reasonable that $\partial Pos(2D_2)/\partial Pos(G)$ is quite different from $Pos(2D_2)/Pos(G)$.

It is worthwhile to compare the temperature dependence of peak position and FWHM broadening of graphite and silicon [39]. Note that if the absolute temperature is used, some ambiguity may exists. For instance, the line shift induced by phonon anharmonicity is 13.8 cm^{-1} (consider the magnitude only), in the range of 4~800 K. This value is much larger than that of Si (~11 cm^{-1}) in the same temperature range. On the other hand, the remaining FWHM dependence only on phonon anharmonicity in graphite is ~1.7 cm^{-1} at 80 K, which is much larger that that (~1.1 cm^{-1}) of silicon. The value of $\Gamma^{an}(800\,K)/\Gamma^{an}(80\,K)$ in graphite is 2.5, while that in silicon is 6.5. Note that the phonon energy for the two modes are significantly different, it is inappropriate to compare them directly using the absolute temperature. To deal with this

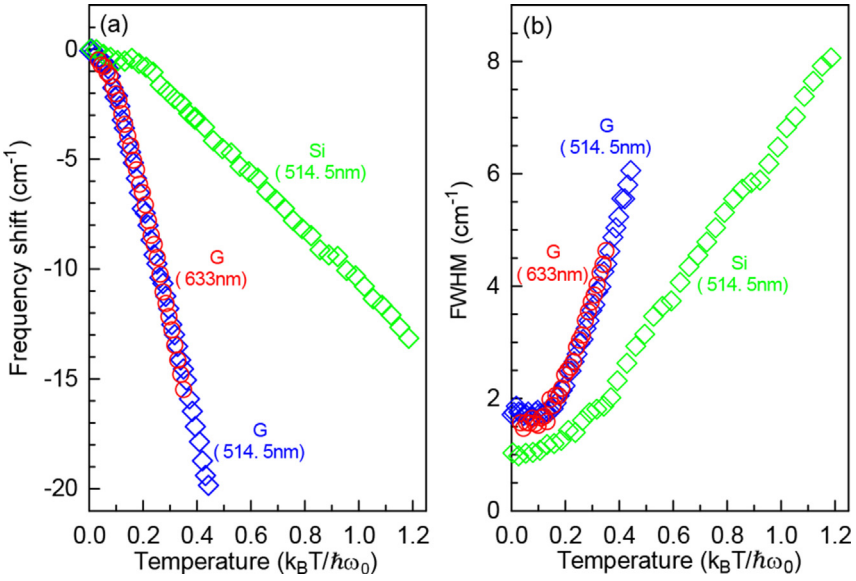

Fig. 5. The comparison of (a) peak position and (b) linewidth broadening with respect to the normalized temperature for the G mode and Si mode. Diamonds are the results measured by the Montana station (4~300 K) and TS1200 stage (300~1000 K) with the 514.5 nm laser. Circles are the results measured by the THMS600 stage (80~800 K) with the 633 nm laser. The contribution from thermal expansion has been excluded in panel (a). The contribution from EPC has been excluded in panel (b). (A colour version of this figure can be viewed online.)

issue, we present the results using the normalized temperature, as shown in Fig. 5(a) and (b). The temperature is normalized as $k_BT/\hbar\omega_0$, where ω_0 represents Pos(G) and Pos(Si) extrapolated at $T = 0K$. Thus, a direct comparison on the temperature dependence of Raman spectra between these two materials can be made. In Fig. 5(a), after subtracting the thermal expansion contributions [3,39,42,43] from the present experimental results, it could be easily seen that Pos(G) in graphite shows a stronger temperature dependence than Pos(Si) in silicon, since the former exhibits a steeper slope than the latter one. Fig. 5(b) shows the FWHM broadening of the two modes with respect to the normalized temperature, with the contribution from EPC being excluded in graphite. Unlike the ambiguity resulted from the use of absolute temperature, in Fig. 5(b), it is readily shown that there is more prominent temperature dependence of phonon anharmonicity of the G mode in graphite than the Si mode in silicon. Within the same normalized temperature range, the increase of FWHM(G) in graphite is actually much larger than FWHM(Si) in silicon. Thus, for both peak position and FWHM, the contribution of phonon anharmonicity is more prominent for the G mode in graphite than the Si mode in silicon.

4. Conclusion

T-dependent Raman spectra of graphene were found to be very sensitive to both samples and detailed experimental conditions, which lead to the diverse results by different groups. To reveal the intrinsic temperature effect of the graphene-based systems, we studied the phonon anharmonicity and EPC in graphite by T-dependent Raman spectroscopy in the temperature range from 4 K to 1000 K. Pos(G) shows a nonlinear dependence on temperature, which is well explained by thermal expansion effect and phonon anharmonicity including both 3-ph and 4-ph scattering processes. As for the FWHM, the G and 2D peaks exhibit different T-dependent behaviors: unlike the 2D peak which shows a linear broadening when temperature increases, the G peak shows a nonlinear dependence on temperature. The intrinsic contribution from phonon anharmonicity and EPC was distinguished. It is found that the contribution of phonon anharmonicity to both peak position and FWHM of the G mode in graphite is more prominent than the Si mode in silicon. Since graphite is a basic material for carbon allotropes, the above results will be very helpful in understanding the mechanism of phonon anharmonicity and EPC in other carbon based materials, such as graphene and carbon nanotubes.

Acknowledgments

We acknowledge the helpful discussion with Prof. A.C. Ferrari and the support from the National Key Research and Development Program of China (Grant No. 2016YFA0301204), the National Natural Science Foundation of China (Grant Nos. 11874350 and 11434010), and Beijing Municipal Science and Technology Commission.

References

[1] A.C. Ferrari, D.M. Basko, Raman spectroscopy as a versatile tool for studying the properties of graphene, Nat. Nanotechnol. 8 (4) (2013) 235–246, https://doi.org/10.1038/nnano.2013.46.
[2] J.B. Wu, M.L. Lin, X. Cong, H.N. Liu, P.H. Tan, Raman spectroscopy of graphene-based materials and its applications in related devices, Chem. Soc. Rev. 47 (2018) 1822–1873, https://doi.org/10.1039/C6CS00915H.
[3] N. Bonini, M. Lazzeri, N. Marzari, F. Mauri, Phonon anharmonicities in graphite and graphene, Phys. Rev. Lett. 99 (17) (2007) 176802, https://doi.org/10.1103/PhysRevLett.99.176802.
[4] F. Bonaccorso, Z. Sun, T. Hasan, A. Ferrari, Graphene photonics and optoelectronics, Nat. Photon. 4 (9) (2010) 611, https://doi.org/10.1038/NPHOTON.2010.186.
[5] A.K. Geim, K.S. Novoselov, The rise of graphene, Nat. Mater. 6 (3) (2007) 183–191, https://doi.org/10.1038/nmat1849.
[6] M. Freitag, M. Steiner, Y. Martin, V. Perebeinos, Z. Chen, J.C. Tsang, et al., Energy dissipation in graphene field-effect transistors, Nano Lett. 9 (5) (2009) 1883–1888, https://doi.org/10.1021/nl803883h.
[7] A.A. Balandin, S. Ghosh, W. Bao, I. Calizo, D. Teweldebrhan, F. Miao, et al., Superior thermal conductivity of single-layer graphene, Nano Lett. 8 (3) (2008) 902–907, https://doi.org/10.1021/nl0731872.
[8] X. Du, I. Skachko, A. Barker, E.Y. Andrei, Approaching ballistic transport in suspended graphene, Nat. Nanotechnol. 3 (2008) 491–C495, https://doi.org/10.1038/nnano.2008.199.
[9] L. Wang, I. Meric, P.Y. Huang, Q. Gao, Y. Gao, H. Tran, et al., One-dimensional electrical contact to a two-dimensional material, Science 342 (2013) 614–617, https://doi.org/10.1126/science.1244358.
[10] X. Li, G. Zhang, X. Bai, X. Sun, X. Wang, E. Wang, et al., Highly conducting graphene sheets and Langmuir-Blodgett films, Nat. Nanotechnol. 3 (2008) 538–542, https://doi.org/10.1126/science.1244358.
[11] I. Calizo, A. Balandin, W. Bao, F. Miao, C. Lau, Temperature dependence of the Raman spectra of graphene and graphene multilayers, Nano Lett. 7 (9) (2007) 2645–2649, https://doi.org/10.1021/nl071033g.
[12] D. Yoon, Y.W. Son, H. Cheong, Negative thermal expansion coefficient of graphene measured by Raman spectroscopy, Nano Lett. 11 (8) (2011) 3227–3231, https://doi.org/10.1021/nl201488g.
[13] S. Linas, Y. Magnin, B. Poinsot, O. Boisron, G.D. Förster, V. Martinez, et al., Interplay between Raman shift and thermal expansion in graphene: temperature-dependent measurements and analysis of substrate corrections, Phys. Rev. B 91 (2015) 075426, https://doi.org/10.1103/PhysRevB.91.075426.
[14] P. Shaina, L. George, V. Yadav, M. Jaiswal, Estimating the thermal expansion coefficient of graphene: the role of graphene–substrate interactions, J. Phys. Condens. Matter 28 (8) (2016) 085301, https://doi.org/10.1088/0953-8984/28/8/085301.
[15] S. Tian, Y. Yang, Z. Liu, C. Wang, R. Pan, C. Gu, et al., Temperature-dependent Raman investigation on suspended graphene: contribution from thermal expansion coefficient mismatch between graphene and substrate, Carbon 104 (2016) 27–32, https://doi.org/10.1016/j.carbon.2016.03.046.
[16] Y.R. Lee, J.X. Huang, J.C. Lin, J.R. Lee, Study of the substrate-induced strain of as-grown graphene on Cu(100) using temperature-dependent Raman spectroscopy: estimating the mode grüneisen parameter with temperature, J. Phys. Chem. C 121 (49) (2017) 27427–27436, https://doi.org/10.1021/acs.jpcc.7b08170.
[17] J. Lin, L. Guo, Q. Huang, Y. Jia, L. Kang, X. Lai, et al., Anharmonic phonon effects in Raman spectra of unsupported vertical graphene sheets, Phys. Rev. B 83 (12) (2011) 1161–1171, https://doi.org/10.1103/physrevb.83.125430.
[18] C. Casiraghi, S. Pisana, K.S. Novoselov, A.K. Geim, A.C. Ferrari, Raman fingerprint of charged impurities in graphene, Appl. Phys. Lett. 91 (23) (2007) 233108, https://doi.org/10.1063/1.2818692.
[19] A. Ferrari, J. Meyer, V. Scardaci, C. Casiraghi, M. Lazzeri, F. Mauri, et al., Raman spectrum of graphene and graphene layers, Phys. Rev. Lett. 97 (18) (2006) 187401, https://doi.org/10.1103/physrevlett.97.187401.
[20] W.J. Zhao, P.H. Tan, J. Liu, A.C. Ferrari, Intercalation of few-layer graphite flakes with fecl3: Raman determination of fermi level, layer by layer decoupling, and stability, J. Am. Chem. Soc. 133 (15) (2011) 5941–5946, https://doi.org/10.1021/ja110939a.
[21] A. Das, S. Pisana, B. Chakraborty, S. Piscanec, S. Saha, U. Waghmare, et al., Monitoring dopants by Raman scattering in an electrochemically top-gated graphene transistor, Nat. Nanotechnol. 3 (4) (2008) 210–215, https://doi.org/10.1038/nnano.2008.67.
[22] S. Pisana, M. Lazzeri, C. Casiraghi, K.S. Novoselov, A.K. Geim, A.C. Ferrari, et al., Breakdown of the adiabatic Born-Oppenheimer approximation in graphene, Nat. Mater. 6 (3) (2007) 198–201, https://doi.org/10.1038/nmat1846.
[23] N. Mounet, N. Marzari, First-principles determination of the structural, vibrational and thermodynamic properties of diamond, graphite, and derivatives, Phys. Rev. B 71 (2005) 205214, https://doi.org/10.1103/PhysRevB.71.205214.
[24] J.W. Jiang, J.S. Wang, B. Li, Thermal expansion in single-walled carbon nanotubes and graphene: nonequilibrium Green's function approach, Phys. Rev. B 80 (2009) 205429, https://doi.org/10.1103/PhysRevB.80.205429.
[25] M. Pozzo, D. Alfè, P. Lacovig, P. Hofmann, S. Lizzit, A. Baraldi, Thermal expansion of supported and freestanding graphene: lattice constant versus interatomic distance, Phys. Rev. Lett. 106 (2011) 135501, https://doi.org/10.1103/PhysRevLett.106.135501.
[26] Z. Moradi, M. Vaezzadeh, M. Saeidi, Temperature-dependent thermal expansion of graphene, Physica A 512 (2018) 81–985, https://doi.org/10.1016/j.physa.2018.08.149.
[27] F. Tuinstra, J.L. Koenig, Raman spectrum of graphite, J. Chem. Phys. 53 (3) (1970) 1126–1130, https://doi.org/10.1063/1.1674108.
[28] N. Everall, J. Lumsdon, D. Christopher, The effect of laser-induced heating upon the vibrational Raman spectra of graphites and carbon fibres, Carbon 29 (2) (1991) 133–137, https://doi.org/10.1016/0008-6223(91)90064-P.
[29] P.H. Tan, Y. Deng, Q. Zhao, W. Cheng, The intrinsic temperature effect of the Raman spectra of graphite, Appl. Phys. Lett. 74 (13) (1999) 1818, https://doi.org/10.1063/1.123096.
[30] P. Giura, N. Bonini, G. Creff, J. Brubach, P. Roy, M. Lazzeri, Temperature evolution of infrared-and Raman-active phonons in graphite, Phys. Rev. B 86 (12)

(2012) 121404, https://doi.org/10.1103/PhysRevB.86.121404.
[31] G. Montagnac, R. Caracas, E. Bobocioiu, F. Vittoz, B. Reynard, Anharmonicity of graphite from UV Raman spectroscopy to 2700 k, Carbon 54 (2013) 68–75, https://doi.org/10.1016/j.carbon.2012.11.004.
[32] M. Balkanski, R. Wallis, E. Haro, Anharmonic effects in light scattering due to optical phonons in silicon, Phys. Rev. B 28 (4) (1983) 1928, https://doi.org/10.1103/PhysRevB.28.1928.
[33] K.S. Novoselov, A.K. Geim, S.V. Morozov, D. Jiang, Y. Zhang, S.V. Dubonos, et al., Electric field effect in atomically thin carbon films, Science 306 (5696) (2004) 666–669, https://doi.org/10.1126/science.1102896.
[34] X.L. Li, W.P. Han, J.B. Wu, X.F. Qiao, J. Zhang, P.H. Tan, Layer-number dependent optical properties of 2D materials and their application for thickness determination, Adv. Funct. Mater. 27 (19) (2017) 1604468, https://doi.org/10.1002/adfm.201604468.
[35] P.H. Tan, Y. Deng, Q. Zhao, Temperature-dependent Raman spectra and anomalous Raman phenomenon of highly oriented pyrolytic graphite, Phys. Rev. B 58 (9) (1998) 5435, https://doi.org/10.1103/physrevb.58.5435.
[36] G. Froehlicher, S. Berciaud, Raman spectroscopy of electrochemically gated graphene transistors: geometrical capacitance, electron-phonon, electron-electron, and electron-defect scattering, Phys. Rev. B 91 (20) (2015) 205413, https://doi.org/10.1103/PhysRevB.91.205413.
[37] F. Huang, K.T. Yue, P. Tan, S.L. Zhang, Z. Shi, X. Zhou, et al., Temperature dependence of the Raman spectra of carbon nanotubes, J. Appl. Phys. 84 (7) (1998) 4022–4024, https://doi.org/10.1063/1.368585.
[38] H. Li, K. Yue, Z. Lian, Y. Zhan, L. Zhou, S. Zhang, et al., Temperature dependence of the Raman spectra of single-wall carbon nanotubes, Appl. Phys. Lett. 76 (15) (2000) 2053–2055, https://doi.org/10.1063/1.126252.
[39] J. Menéndez, M. Cardona, Temperature dependence of the first-order Raman scattering by phonons in Si, Ge, and α-Sn: anharmonic effects, Phys. Rev. B 29 (4) (1984) 2051, https://doi.org/10.1103/PhysRevB.29.2051.
[40] C. Thomsen, S. Reich, Double resonant Raman scattering in graphite, Phys. Rev. Lett. 85 (24) (2000) 5214, https://doi.org/10.1103/physrevlett.85.5214.
[41] R. Saito, A. Jorio, A. Souza Filho, G. Dresselhaus, M. Dresselhaus, M. Pimenta, Probing phonon dispersion relations of graphite by double resonance Raman scattering, Phys. Rev. Lett. 88 (2) (2001) 027401, https://doi.org/10.1103/physrevlett.88.027401.
[42] Y. Okada, Y. Tokumaru, Precise determination of lattice parameter and thermal expansion coefficient of silicon between 300 and 1500 K, J. Appl. Phys. 56 (2) (1984) 314–320, https://doi.org/10.1063/1.333965.
[43] T. Middelmann, A. Walkov, G. Bartl, R. Schodel, Thermal expansion coefficient of single-crystal silicon from 7 K to 293 K, Phys. Rev. B 92 (17) (2015) 174113, https://doi.org/10.1103/PhysRevB.92.174113.